J. Plasma Physics (2012), vol. 78, part 4, pp. 421–427. © Cambridge University Press 2012
doi:10.1017/S002237781200027X

Electromagnetic emission from laser wakefields in underdense magnetized plasmas

Z. D. HU[1], Z. M. SHENG[1,2], W. J. DING[1], W. M. WANG[1], Q. L. DONG[1] and J. ZHANG[1,2]

[1]Beijing National Laboratory of Condensed Matter Physics, Institute of Physics, CAS, Beijing, 100190, China
[2]Key Laboratory for Laser Plasmas (Ministry of Education) and Department of Physics, Shanghai Jiaotong University, Shanghai, 200240, China
(zmsheng@aphy.iphy.ac.cn)

(Received 30 September 2011; revised 5 January 2012; accepted 7 February 2012; first published online 15 March 2012)

Abstract. The laser wakefield structure in a magnetized underdense plasma is studied analytically and numerically. Because of the DC magnetic field perpendicular to the laser propagation direction, an electromagnetic component appears in addition to the normal electrostatic component. This electromagnetic component can transmit partially into vacuum at the plasma–vacuum boundary as shown by particle-in-cell simulation. It is found that the emission has components both at the fundamental plasma frequency and its harmonics if the wakefield is driven at a high amplitude. Comparing with the emission at the plasma frequency, the harmonic emission depends weakly upon the density profile at plasma–vacuum boundary and it can pass through the boundary almost without energy loss, providing a new method for the diagnostic of wakefields.

1. Introduction

A wakefield is usually an electrostatic wave driven by a laser pulse or a charged particle bunch in plasmas (Sprangle et al., 1988, 1990). Once the wakefield is driven at a large amplitude, it has lots of application prospects, such as high-gradient electron acceleration (Pukhov and Meyer-ter Vehn, 2002; Faure et al., 2006; Leemans et al., 2006), X-ray radiation (Kostyukov et al., 2003; Rousse et al., 2004), and terahertz radiation (Sheng et al., 2005). The wakefield structure has been measured using an interferometric technique (Siders et al., 1996; Matlis et al., 2006), and the wakefield strength has been measured indirectly by the tomographic diagnosis method (Hsieh et al., 2006). Here we propose another diagnostic of the wakefield structure by measuring the electromagnetic emission of the wakefield.

It is well known that the unmagnetized wakefield is a pure longitudinal wave in which the net current is vanished, since the real current and the displacement current cancel each other. Therefore, the direct conversion from wakefields into electromagnetic emissions does not happen. By introducing an inhomogeneous plasma, it has been shown that the wakefield can be partially converted into electromagnetic emission via linear mode conversion (Sheng et al., 2005). But this emission is usually found in the backward direction and has a broad emission spectrum. Alternatively, an external DC magnetic field applied in the transverse direction makes the wakefield partially electromagnetic even in homogeneous plasma. This is due to the transverse motion of electrons under the Lorenz force, inducing a transverse current and making the electromagnetic emission possible. Previous studies have already demonstrated the key roles that the DC magnetic field can play in the electromagnetic radiation (Yoshii et al., 1997; Spence et al., 2001; Yugami et al., 2002; Wu et al., 2007). For example, Yoshii et al. (1997) has investigated the radiation using the dispersion relation of an extraordinary wave for weakly relativistic wakefields. Here we provide a theoretical model for the wakefield structure excited in magnetized plasmas for both weakly and highly relativistic cases, including the obliquely magnetized condition. It is shown that by measuring the electromagnetic emission at the plasma–vacuum boundary both at the fundamental and high harmonics, one can obtain the wakefield strength and the plasma density. This provides a new method for the wakefield diagnostic.

This paper is organized as follows. In Sec. 2, a theoretical model for the magnetized wakefield is presented. In Sec. 3, we give one-dimensional (1D) particle-in-cell (PIC) simulation results to confirm this model. In order to investigate radiation through the plasma–vacuum boundary, the effect of plasma density gradients at the boundary is also discussed. Furthermore, the diagnosis of wakefields using the higher harmonic radiation is presented. Preliminary 2D PIC simulation is also shown. Finally, the paper concludes with some discussions in Sec. 4.

2. Analytical model

Here we consider that a laser pulse propagates perpendicularly into the magnetized plasmas along the x-direction with polarization in the z-direction. The duration of the laser pulse is short enough so that the response of ions can be ignored. Firstly, we consider the external magnetic field B_0 in the z-direction. The laser–plasma interaction can be described by the vector potential equation, Poisson's equation, continuity equation, and momentum equations for a cold electron fluid as follows:

$$\left(\nabla^2 - \frac{1}{c^2}\frac{\partial^2}{\partial t^2}\right)\boldsymbol{a} = k_p^2(1+n)\boldsymbol{\beta}, \tag{2.1}$$

$$\nabla^2\phi = k_p^2 n, \tag{2.2}$$

$$\frac{1}{c}\frac{\partial n}{\partial t} + \nabla\cdot[(1+n)\boldsymbol{\beta}] = 0, \tag{2.3}$$

$$\frac{1}{c}\frac{d}{dt}(\gamma\boldsymbol{\beta}) = \frac{1}{c}\frac{\partial \boldsymbol{a}}{\partial t} + \nabla\phi - \boldsymbol{\beta}\times(\nabla\times\boldsymbol{a} + k_p\boldsymbol{b}), \tag{2.4}$$

where c is the velocity of light, the vector potential a, normalized by $m_e c^2/e$, is associated with electric fields of the laser pulse and the transverse field, the scalar potential is normalized by $m_e c^2/e$, the perturbation of electron density n by the initial density n_0, and the velocity β by c. Also, in these equations, $b = \omega_c/\omega_p = eB_0/m_e\omega_p c$ stands for the external DC magnetic field parameter, $k_p = \omega_p/c = (4\pi n_0 e^2/m_e)^{1/2}/c$, and $\gamma = [(1+a_L^2)/(1-\beta_x^2-\beta_y^2)]^{1/2}$ is the relativistic factor, where a_L is the normalized laser intensity. The longitudinal wakefield E_x and the transverse component $E_\perp$ are described by ϕ and a, respectively. Note that there is $\omega_c \ll \omega_p$ under normal laboratory conditions (for example, $\omega_c/\omega_p \sim 10^{-2}$ for $B_0 = 10$T in atmospheric pressure), and the wakefield frequency does not show an obvious shift.

For the 1D geometry, we have found that (Hu et al. in press) the longitudinal wave E_x is not affected obviously by the external magnetic field and still can be described by the equations given by Sprangle et al. (1988, 1990). Besides, the external magnetic field B_0 couples the electron longitudinal motion with the transverse motion, leading to a new transverse component E_y, which follows the scaling law,

$$E_y = -b\beta_g\frac{\partial E_x}{\partial\xi} \tag{2.5}$$

in both weakly relativistic and highly relativistic regime, where E_x and E_y are normalized by $m_e\omega_p c/e$. Here an algebraic transformation ($\xi_0 = x - v_g t, \tau = t$) is performed, where $v_g = c(1-\omega_p^2/\omega_0^2)^{1/2}$ is the group velocity of the laser pulse with a frequency of ω_0, and $\xi = k_p\xi_0, \beta_g = v_g/c$.

It must be emphasized that the electromagnetic field E_y has a non-zero group velocity, though its oscillation frequency is equal to the electron plasma frequency. Because of the external magnetic field, E_x and E_y are coupled into one mode: the extraordinary mode, following the same dispersion relation: $c^2k^2 = \omega^2 - \omega_p^2[(\omega^2-\omega_p^2)/(\omega^2-\omega_h^2)]$, where $\omega_h = [\omega_p^2+\omega_c^2]^{1/2}$. At the point $\omega = \omega_p$, the group velocity $V_g = d\omega/dk = (\omega_c^2/\omega_h^2)c$. Consequently, this non-zero group velocity allows the transmission of E_y at the plasma–vacuum boundary, making the electromagnetic emission possible, as shown later in Sec. 3.

In the following, we add some discussion of the wakefield structure with an oblique DC magnetic field $\boldsymbol{B_0} = \boldsymbol{B_{z0}} + \boldsymbol{B_{x0}}$. In this case, in addition to the transverse component E_y caused by B_{z0}, another component E_z appears under the Lorenz force $\boldsymbol{v_y}\times\boldsymbol{B_{x0}}$. In order to estimate the value of E_z, one can make some simple estimations. The potential equation and momentum equation can be written as

$$(1-\beta_g^2)\frac{\partial^2}{\partial\xi^2}a_{y,z} = (1+n)\beta_{y,z}, \tag{2.6}$$

$$-\beta_g\frac{\partial\beta_g}{\partial\xi} = -\beta_g\frac{\partial a_z}{\partial\xi} + \beta_x\frac{\partial a_z}{\partial\xi} + b_x\beta_y, \tag{2.7}$$

where $b_x = b\cos\theta$ with $b = eB_0/m_e\omega_p c$. Here we take $a_{y,z} \sim \exp(i\xi)$, $\beta_z \sim \exp(i\xi)$, then (2.6) and (2.7) can be written as

$$(1-\beta_g^2)a_{y,z} = -(1+n)\beta_{y,z}, \tag{2.8}$$

$$-\beta_g\beta_z = (\beta_x - \beta_g)a_z - ib_x\beta_y. \tag{2.9}$$

Through the algebraic transformation and linear approximation $\frac{\partial}{\partial\xi} = i\xi$, (2.3) can be simplified as

$$(1+n)\beta_x = n\beta_g. \tag{2.10}$$

Combining (2.8)–(2.10), we get

$$a_z = \frac{ib_x(1-\beta_g^2)}{\beta_g(2-\beta_g^2)}a_y, \tag{2.11}$$

and E_z and E_y are related to each other in the same way as a_z and a_y. For $|b_x| \ll 1, 1-\beta_g^2 \ll 1$, a_z is a second-order small quantity, which indicates that E_z is negligible in the wake. Since E_y and E_z are only weakly coupled, E_y is not significantly changed in the presence of E_z and still determined by B_z, following

$$E_y = -b\beta_g\frac{\partial E_x}{\partial\xi}\sin\theta. \tag{2.12}$$

Therefore, one can conclude that the magnetic field along the longitudinal axis has little contribution to the electromagnetic component.

3. Results from simulations

3.1. Comparison between the analytical results and simulations

In order to test the model outlined above, we have made a series of 1D PIC simulations. The laser pulse propagates in the x-direction. The plasma density is $n_0 = 10^{-4}n_c$, corresponding to a plasma wavelength $\lambda_p = 100\lambda_0$, where $n_c = 1.1\times10^{21}\,(\mu m/\lambda_0)^2\mathrm{cm}^{-3}$ is the

https://doi.org/10.1017/S002237781200027X Published online by Cambridge University Press

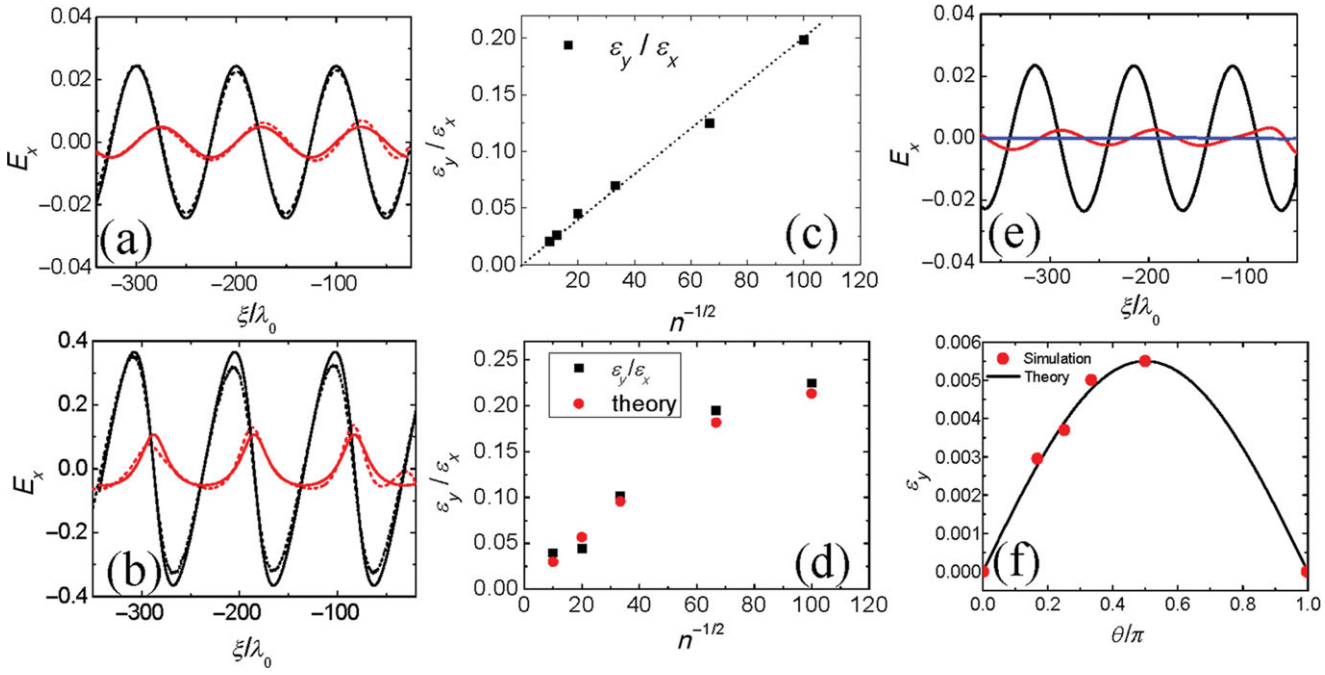

Figure 1. (Color online) The wakefield excited in perpendicularly magnetized plasmas obtained from 1D simulations (dashed curves) and theoretical calculations (solid curves) for (a) $a_L = 0.5$ and (b) $a_L = 2.0$. The black lines show the longitudinal field and red lines show the transverse field. Ratios of normalized amplitudes ε_y and ε_x for different plasma densities with (c) $a_L = 0.5$ and (d) $a_L = 2.0$. The laser durations are $\tau = 10T_0$. (e) The magnetized wakefield obtained from simulation for the DC magnetic field pointing in the angle $\theta = \pi/4$, where the black, red, and blue lines show E_x, E_z, and E_y, respectively (E_y has been multiplied by a factor of 2). (f) Normalized amplitude of E_y as a function of θ.

critical density for a laser pulse with wavelength λ_0. For $\lambda_0 = 1\,\mu m$, we have $n_0 = 1.1 \times 10^{17}\,\mathrm{cm}^{-3}$, corresponding to a plasma frequency $f = \omega_p/2\pi = 2.98\,\mathrm{THz}$. In the following simulations, we always take $n_0 = 10^{-4}n_c$, $\lambda_0 = 1\,\mu m$, as well as $B_0 = 22$ T, corresponding to $b = 0.2$, and the amplitudes of electric fields are all normalized by $m_e\omega_p c/e$. The pulse has a Gaussian envelope with a duration of $\tau = 5\ T_0$, where T_0 is the laser cycle.

Figures 1(a) and (b) plot the longitudinal and transverse fields with B_0 pointing in the z-direction, which shows a good agreement between the 1D simulation and the analytical results in both weakly relativistic and highly relativistic regimes.

A series of simulation results for different plasma densities are also presented here. Ratios of ε_y and ε_x, which are normalized amplitudes of E_y and E_x, are plotted as a function of $n^{-1/2}$ in Figs. 1(c) and (d), where n is the plasma density ranging from 10^{17} to 10^{19} cm^{-3}, normalized by the critical density n_c. According to (2.5) and the expression of b, one can find that $\varepsilon_y/\varepsilon_x \infty n^{-1/2}$ in the linear regime. This linear relationship has been shown in Fig. 1(c). Although in the relativistic regime the nonlinear feature starts to appear, the simulation results still agree well with theoretical results, as shown in Fig. 1(d).

Figure 1(e) shows the wakefield with B_0 in the direction of 45° to x-direction. The laser intensity is $a_L = 0.5$, and the pulse duration is $\tau = 5T_0$. Clearly, the electric field E_z is nearly zero compared with E_x and E_y, which verifies the above statement. Figure 1(f) plots the normalized amplitude of E_y as a function of θ, which is the angle between B_0 and the x-direction. The simulation results match the theoretical result very well. Obviously, when the magnetic field is parallel to the x-axis, there is no electromagnetic field at all.

3.2. *The wakefield emission through the boundary*

In order to investigate the emission of the wakefield through the plasma–vacuum boundary in the forward direction, we give some examples via 1D PIC simulation, as shown in Fig. 2, where both weakly relativistic cases (left column) and highly relativistic cases (right column) are plotted at $t = 15T_0$, with $a_L = 0.5$ and 2.0, respectively. The magnetic field is simply along the z-direction. In case (a) there is an abrupt boundary at $x = 450\lambda_0$, while in cases (b) and (c) the density declines linearly from n_0 at $x = 450\lambda_0$ to zero over the length λ_p and $2\lambda_p$, respectively. Other conditions are the same as above. In each case, the longitudinal field E_x vanishes in the vacuum, since there is no charge separation there. In contrast, the transverse field E_y can transmit through the boundary as electromagnetic emission. The transmission loss of E_y is due to the evanescent layer in the region $\omega_h(x) < \omega_p < \omega_R(x)$, where $\omega_R(x) = \{\omega_c + [\omega_c^2 + 4\omega_p(x)^2]^{1/2}\}/2$ (Chen, 2007). It is obvious that the transmission loss increases when increasing the length of the inhomogeneous density region, as shown in Fig. 2, which is similar to those observed by Yoshii et al. (1997) .

https://doi.org/10.1017/S002237781200027X Published online by Cambridge University Press

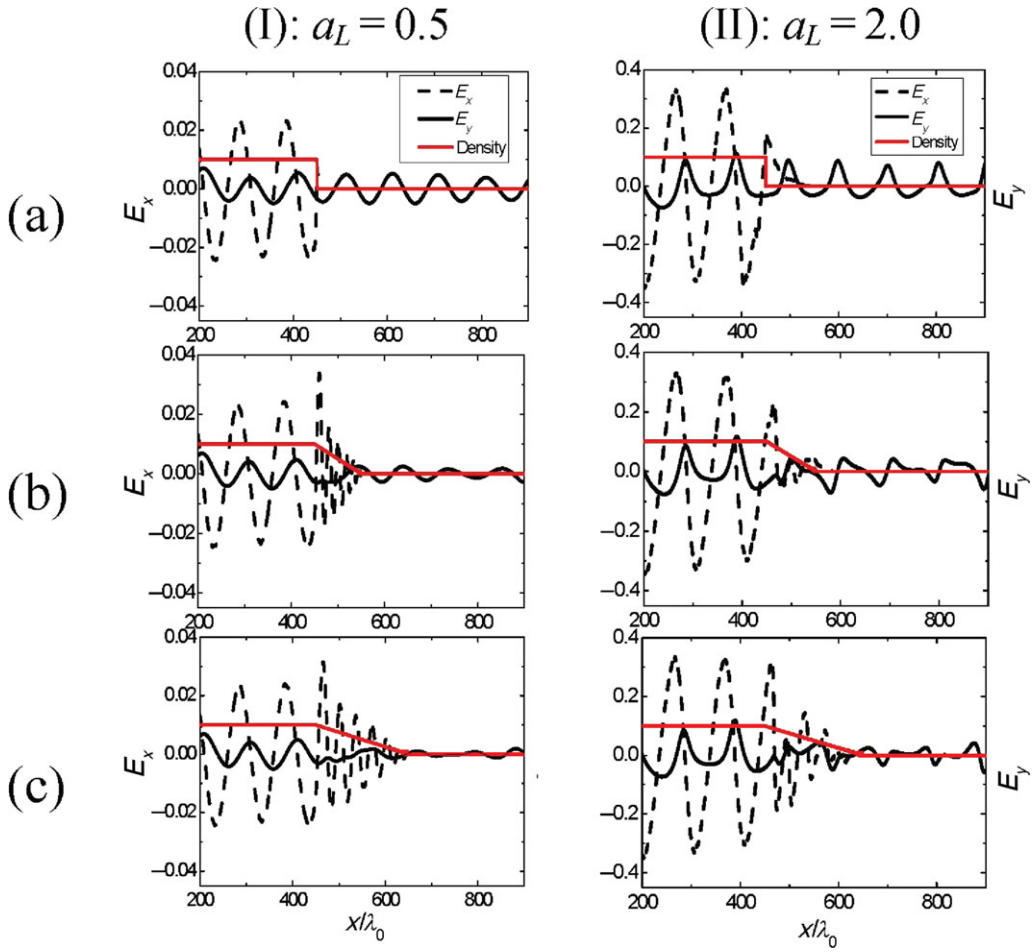

Figure 2. (Color online) The transmission of magnetized wakefields (the dashed and solid black curves represent the E_x and E_y, respectively) through the plasma–vacuum boundary for $a_L = 0.5$ (left column) and $a_L = 2.0$ (right column). The red curve represents the initial density profile. The density n has been multiplied by an additional factor of 10^2 for $a_L = 0.5$, and 10^3 for $a_L = 2.0$. In case (a), there is a sharp boundary at $x = 450\lambda_0$. In cases (b) and (c), the plasma density declines linearly form $n = n_0$ at $x = 450\lambda_0$ to $n = 0$ at $x = 550\lambda_0$ and $650\lambda_0$, respectively.

Note that the electromagnetic wave exhibits an obvious variation in its waveform when the driving laser intensity is increased to a high level, which implies the presence of higher harmonic components. Because $2\omega_p > \omega_R(x)$ in the inhomogeneous region, the harmonic waves are not influenced by the evanescent layer and reveal themselves ultimately in the vacuum without loss, though the fundamental wave has decreased in its amplitude. Figure 3(a) shows the temporal profile of the emission E_y, and the parameters are the same as for Fig. 2(c) for $a_L = 2.0$. For the nonlinear feature and the decay of the fundamental emission, the waveform exhibits strong irregularity. The spectrum of E_y in homogeneous plasmas (solid curves) and the vacuum region (dashed curves) for $a_L = 2.0, L = 2\lambda_p$ are presented in Fig. 3(b). One can easily note that the fundamental component in the vacuum region is reduced significantly as compared with that in the plasma region, while the second and higher harmonic components have little decrease. As a result, the second harmonic component becomes comparable with the fundamental one, resulting in the variation of the waveform.

3.3. *Diagnostic of wakefields*

As mentioned above, the external magnetic field leads to a new transverse component E_y in the wake, while the wakefield E_x is not significantly changed; moreover, the higher harmonic components of the transverse field can transmit out of plasmas with little energy loss. This provides a possibility to use the higher harmonic wave emitted out of plasmas as a tool for the wakefield diagnosis. An example is shown in Fig. 4, which compares the measured harmonic amplitudes in vacuum as a function of wakefield amplitudes in the homogenous plasma region away from the boundary when there are different plasma density scale lengths at the plasma–vacuum boundary. $E_{y-n\omega}$ is the maximum amplitude of the emission after passing through a high-pass filter with a cutoff frequency of ω_p, and $E_{y-2\omega}$ is the second harmonic amplitude of the emission. As expected, the harmonic amplitude measured in the vacuum does not much depend upon the plasma density profile at the plasma–vacuum boundary. With the increase of the wakefield amplitude, the harmonic components get more and more proportion, resulting in a slow-down

https://doi.org/10.1017/S002237781200027X Published online by Cambridge University Press

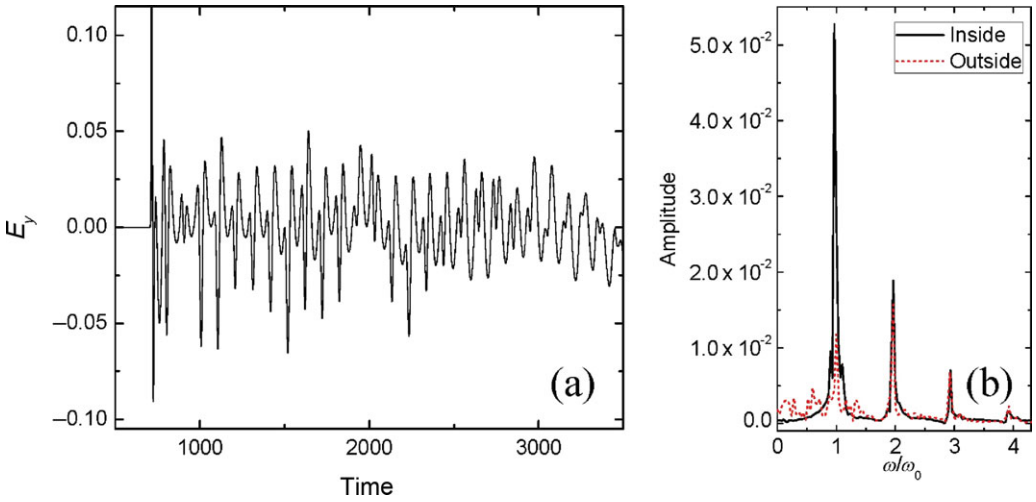

Figure 3. (Color online) (a) The temporal profile of the electromagnetic emission. (b) The spectra of E_y in the homogeneous plasma region (solid curve) and in vacuum (dashed curve) for the incident laser amplitude $a_L = 2.0$ and the length of the inhomogeneous plasma, $L = 2\lambda_p$.

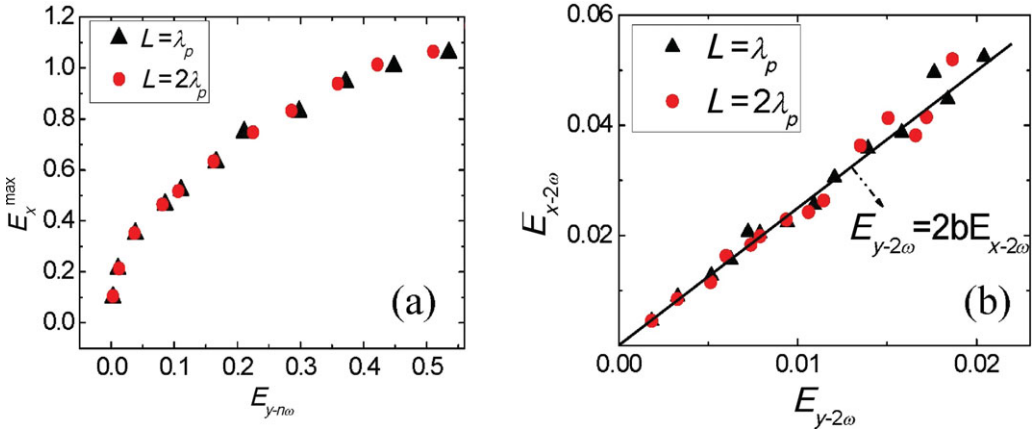

Figure 4. (Color online) (a) Normalized maximum amplitude of the wake $E_x^{\max}$ as a function of $E_{y-n\omega}$; (b) Normalized amplitude of the 2nd harmonic component of the wake $E_{x-2\omega}$ as a function of $E_{y-2\omega}$. The length of the inhomogeneous region is $L = \lambda_p$ (black triangles) and $L = 2\lambda_p$ (red circles).

enhancement of $E_x^{\max}$, as seen in Fig. 4(a). Figure 4(b) shows that the second hamonic amplitudes $E_{y-2\omega}$ and $E_{x-2\omega}$ follow a linear relationship $E_{y-2\omega} = 2bE_{x-2\omega}$, where the values of $E_{x-2\omega}$ and $E_{y-2\omega}$ are obtained through the Fourier analysis. This relationship is consistent with (2.5) too. Figure 5 shows the wakefield in plasmas and temporal profile of the corresponding emission when the wave breaking occurs. Unlike the case in Fig. 3(a), the emission in Fig. 5(b) has only two sharp peaks, after which the signal decreases rapidly and becomes irregular, indicating the presence of wave-breaking. Therefore, the wave-breaking can be detected from the vanishing of the peak structure in the emission. Moreover, since the fundamental frequency of E_y is equal to ω_p, this emission can also provide the information of the plasma density.

3.4. 2D PIC simulation

In order to testify the availability of the above-discussed theory, a 2D PIC simulation result is also presented here. Figure 6 shows the magnetized wakefield when a p-polarized laser pulse propagates in a plasma with density $n_0 = 10^{-2}n_c$. The normalized laser amplitude is 0.5, and the laser duration is $\tau = 5T_0$. The waist of the pulse is $15\lambda_0$. The external magnetic field is along the y-direction, and $B_0 = 22$ T. Figure 6 shows the distribution of the longitudinal field E_x and the transverse field E_z that is induced by B_y. Like the 1D case, the longitudinal field has little change compared to the unmagnetized condition; moreover, the transverse and longitudinal fields still remain at a phase difference of $\pi/2$. The ratio of amplitudes is $\varepsilon_z/\varepsilon_x = 1.82 \times 10^{-2}$, slightly smaller than 0.02, which is the 1D theoretical result. Through a sharp boundary at $x = 28\lambda$, the longitudinal field no longer exits, while the field E_z can still transmit into the vacuum continuously. Therefore, the 1D theory is still applicable here in the linear regime.

It should be pointed out that in the highly nonlinear regime the laser wakefield front is curved and the curvature of the constant phase surfaces increases with

https://doi.org/10.1017/S002237781200027X Published online by Cambridge University Press

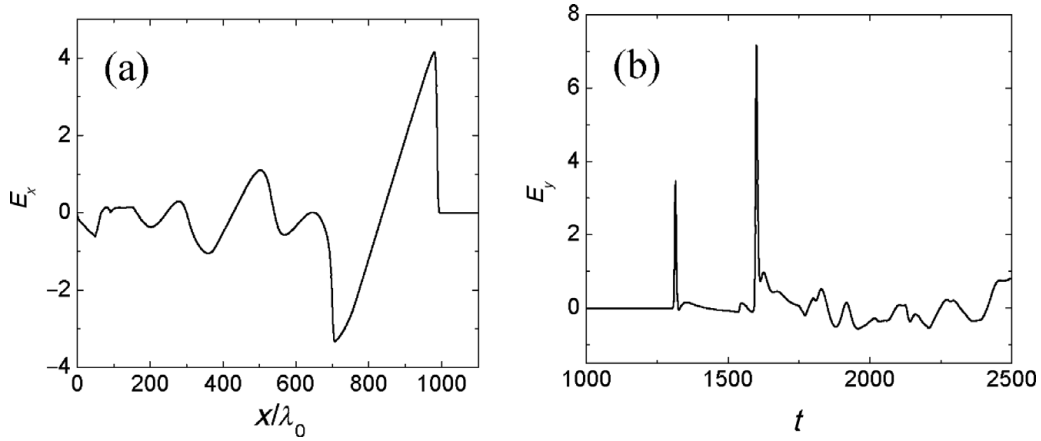

Figure 5. (a) Snapshot of the wakefield E_x at $t = 1000$ T from 1D PIC simulation; (b) temporal profile of the emitted pulse through the right boundary.

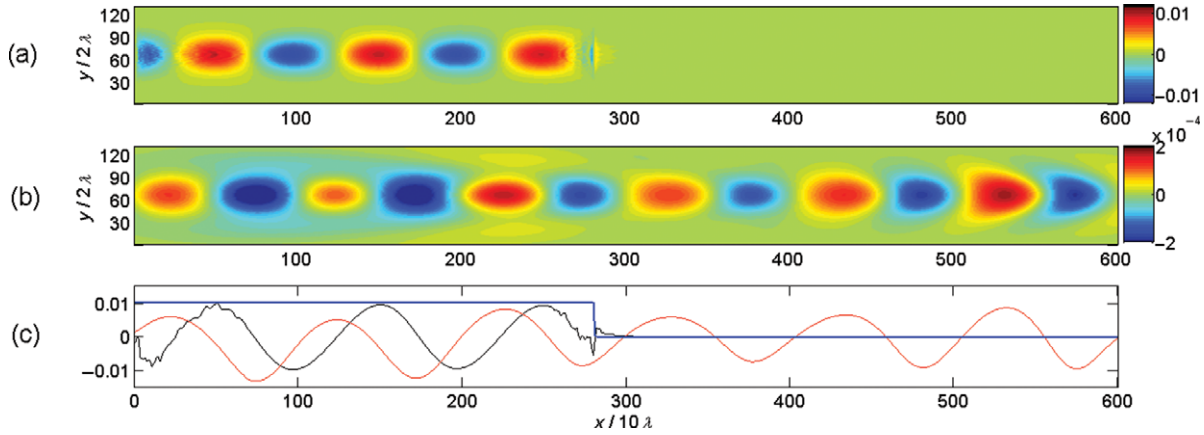

Figure 6. (Color online) Snapshot of (a) the longitudinal field E_x and (b) the transverse field E_z in 2D PIC simulation; (c) the field E_x (the black curve), E_z (the red curve), and the normalized plasma density n_0/n_c (the blue line); the value of E_z has been multiplied by the factor 1.0/0.02.

distance from the pulse because of the relativistic effect (Bulanov et al., 1997). In the meanwhile, a quasi-static magnetic field is produced in the azimuthal direction (Sheng et al., 1998). In the wave-breaking regime, a bubble structure is formed (Pukhov and Meyer-ter Vehn, 2002; Lu et al., 2006). Therefore in the nonlinear and wave-breaking regime, the effect of the transverse DC magnetic field as well as the transmission of the radiation may be somehow different from the pure 1D case. This will be the topic of further studies.

4. Conclusions and discussions

In summary, we have presented a theoretical model for the 1D wakefield driven by a short laser pulse in underdense plasmas in the presence of a strong DC magnetic field. Because of this magnetic field pointing in the transverse direction, a transverse component E_y associated with the longitudinal wakefield E_x appears, while E_x remains almost unchanged. The transverse component mainly results from the effect of B_0, which lies along the transverse direction, whereas the effect of the longitudinal DC magnetic field is not obvious. The transverse field E_y follows a simple relation with the longitudinal field E_x: $E_y = -b\beta_g \frac{\partial E_x}{\partial \xi} \sin\theta$. These results are well confirmed by PIC simulation.

Numerical simulations show that the transverse component E_y can transmit into the vacuum as electromagnetic emission. Moreover, in contrast to the fundamental emission, the higher harmonic components have little energy loss when passing through the boundary. This makes it possible to use the harmonic emission as a diagnostic tool for wakefields without significant boundary effects. The simulation results confirm this possibility. Hence, the harmonic emission provides a new diagnostic for the wakefield structure, such as the amplitude, the harmonic components, the frequency, and even wave-breaking.

Acknowledgments

This work was supported by the National Natural Science Foundation of China (Grants No. 11075105, 10947108, 11121504) and the National Basic Research Program of China (No. 2009GB105002).

https://doi.org/10.1017/S002237781200027X Published online by Cambridge University Press

References

Bulanov, S. V., Pegoraro, F., Pukhov, A. M. and Sakharov, A. S. 1997 Transverse-wake wave breaking. *Phys. Rev. Lett*. **78**, 4205–4208.

Chen, F. F. 2007 *Introduction to Plasma Physics*. New York: Plenum Press.

Faure, J., Rechatin, C., Norlin, A., Lifschitz, A., Glinec, Y. and Malka, V. 2006 Controlled injection and acceleration of electrons in plasma wakefields by colliding laser pulses. *Nature* **444**, 737–739.

Hsieh, C. T., Huang, C. M., Chang, C. L., Ho, Y. C., Chen, Y. S., Lin, J. Y., Wang, J. and Chen, S. Y. 2006 Tomography of injection and acceleration of monoenergetic electrons in a laser-wakefield accelerator. *Phys. Rev. Lett*. **96**, 095001.

Hu, Z. D., Sheng, Z. M., Ding, W. J., Wang, W. M., Dong, Q. L. and Zhang, J. in press Electromagnetic emission from laser wakefields driven in magnetized underdense plasmas. *Plasma Sci. Technol*.

Kostyukov, I., Kiselev, S. and Pukhov, A. 2003 X-ray generation in an ion channel. *Phys. Plasmas* **10**, 4818–4828.

Leemans, W. P., Nagler, B., Gonsalves, A. J., Toth, C., Nakamura, K., Geddes, C. G. R., Esarey, E., Schroeder, C. B. and Hooker, S. M. 2006 Gev electron beams from a centimetre-scale accelerator. *Appl. Phys.* B **2**, 696–699.

Lu, W., Huang, C., Zhou, M., Mori, W. B. and Katsouleas, T. 2006 Nonlinear theory for relativistic plasma wakefields in the blowout regime. *Phys. Rev. Lett*. **96**, 165002.

Matlis, N. H., Reed, S., Bulanov, S. S., Chvykov, V., Kalintchenko, G., Matsuoka, T., Rousseau, P., Yandanovsky, V., Maksimchuk, A., Kalmykov, S. et al. 2006 Snapshots of laser wakefields. *Nat. Phys*. **2**, 749–753.

Pukhov, A. and Meyer-ter Vehn, J. 2002 Laser wake field acceleration: the highly non-linear broken-wave regime. *Appl. Phys.* B **74**, 355–361.

Rousse, A., Phuoc, K. T., Shah, R., Pukhov, A., Lefebvre, E., Malka, V., Kiselev, S., Burgy, F., Rousseau, J., Umstadter, D. et al. 2004 Production of a kev x-ray beam from synchrotron radiation in relativistic laser-plasma interaction. *Phys. Rev. Lett*. **93**, 135005.

Sheng, Z. M., Meyer-ter Vehn, J. and Pukhov, A. 1998 Analytic and numerical study of magnetic fields in the plasma wake of an intense laser pulse. *Phys. Plasmas* **5**(10), 3764–3773.

Sheng, Z. M., Mima, K. and Zhang, J. 2005 Powerful terahertz emission from laser wake fields excited in inhomogeneous plasmas. *Phys. Plasmas* **12**, 123103.

Siders, C. W., Le Blanc, S. P., Fisher, D., Tajima, T., Downer, M. C., Babine, A., Stepanov, A. and Sergeev, A. 1996 Laser wakefield excitation and measurement by femtosecond longitudinal interferometry. *Phys. Rev. Lett*. **76**, 3570–3573.

Spence, N., Katsouleas, T., Muggli, P., Mori, W. B. and Hemker, R. 2001 Simulations of cerenkov wake radiation sources. *Phys. Plasmas* **8**(11), 4995–5005.

Sprangle, P., Esarey, E. and Ting, A. 1990 Nonlinear interaction of intense laser pulses in plasmas. *Appl. Phys. Lett*. **41**, 4463–4469.

Sprangle, P., Esarey, E., Ting, A. and Joyce, G. 1988 Laser wakefield acceleration and relativistic optical guiding. *Appl. Phys. Lett*. **53**, 2146–2148.

Wu, H. C., Sheng, Z. M., Dong, Q. L., Xu, H. and Zhang, J. 2007 Powerful terahertz emission from laser wakefields in inhomogeneous magnetized plasmas. *Phys. Rev*. E **75**, 016407.

Yoshii, J., Lai, C. H., Katsouleas, T., Joshi, C. and Mori, W. B. 1997 Radiation from cerenkov wakes in a magnetized plasma. *Phys. Rev. Lett*. **79**, 4194–4197.

Yugami, N., Higashiguchi, T., Gao, H., Sakai, S., Takahashi, K., Ito, H., Nishida, Y. and Katsouleas, T. 2002 Experimental observation of radiation from cherenkov wakes in a magnetized plasma. *Phys. Rev. Lett*. **89**, 065003.

https://doi.org/10.1017/S002237781200027X Published online by Cambridge University Press